Journal of Applied Polymer Science

Influences of Different Gravity Environments on the Curing Process and Cured Products of Carbon-Nanotube-Reinforced Epoxy Composites

Defeng Li,[1,2] Yuyan Liu,[1] Youshan Wang,[2] Hongjun Kang,[1] Lei Wang,[1] Huifeng Tan[2]

[1]School of Chemical Engineering and Technology, Harbin Institute of Technology, Harbin 150001, China

[2]National Key Laboratory of Science and Technology on Advanced Composites in Special Environments, Harbin Institute of Technology, Harbin 150080, China

Correspondence to: Y. Liu (E-mail: liuyy@hit.edu.cn) and Y. Wang (E-mail: wangys@hit.edu.cn)

ABSTRACT: The influences of different gravity environments on the curing process and the cured products of carbon-nanotube-reinforced epoxy composites were investigated in this study. Different gravity environments were simulated with a superconducting magnet on the basis of which resin matrix composites with different amino-functionalized multiwalled carbon nanotube (NH_2-MWCNT) concentrations of 0.1, 0.3, 0.5, and 1 wt % were tested. Fourier transform infrared spectroscopy, differential scanning calorimetry, dynamic mechanical analysis, thermomechanical analysis (TMA), thermogravimetric analysis, scanning electron microscopy, transmission electron microscopy, and three-point bending tests were used to analyze the characteristics of different curing processes and cured products. From the results, we observed that the curing rate of the epoxy composites was influenced by different gravity values, and there was anisotropy in the NH_2-MWCNT-reinforced epoxy composites cured in the simulated microgravity environment. More effects of gravity on the curing process and cured products could be obtained through detailed experiments and discussion; this is important and fundamental for improving and enhancing the properties of composite materials used in different gravity environments. © 2014 Wiley Periodicals, Inc. J. Appl. Polym. Sci. **2015**, *132*, 41413.

KEYWORDS: composites; crosslinking; gels; mechanical properties; microscopy

Received 3 May 2014; accepted 18 August 2014

DOI: 10.1002/app.41413

INTRODUCTION

Epoxy resins are widely used in almost every field, including in construction materials, the automobile industry, adhesives, coatings, aerospace applications, and electronic circuit board laminates,[1–3] because of their high strength and stiffness, high adhesion, dimensional stability, good chemical and corrosion resistances, low shrinkage, low cost, ease of processing, low specific weight, and long pot-life period.[4–8] Studies of epoxy resin have mainly been concerned with the reaction mechanism,[9,10] curing kinetics,[11,12] properties of shape memory,[13,14] toughening modification and epoxy matrix composites,[15–19] and so on. Among previous studies, big-scale resin materials and resin–matrix composites have been developing rapidly in recent years because other materials, such as metal materials, are difficult to build on a big scale in space. Studies have shown that polymer polymerization is the best way to fabricate a hard space structure; this can also break up the limits of the structure and the size of the space environment laboratory and the space station.[20,21] Many experiments are affected by the terrestrial gravity because of its obvious influences on the sedimentation of polymeric microglobules, and the convection of heat and the concentration.[22–25] Sedimentation and convection during the curing process will cause heat concentration in the lower part of the resin matrix samples, especially for large-scale samples. Under this circumstance, different temperatures in different parts of one sample cause differences in the curing degree (α) and, thus, generate stress concentration; this imposes serious effects on the performance of the material and even leads to the invalidation of large-scale samples.

Carbon nanotubes (CNTs), with small dimensions and high aspect ratios, are considered to be reinforcements to the polymer matrix because of their remarkable physical, chemical, and electrical properties.[26–32] As an important component of high-functional composites, resin matrix composites have been broadly introduced and applied in special requirements fields, such as aviation, marine fields, and railways, where materials with high strength, dimensional stability, low density, and high corrosion resistance are required.[33–35] Among all of the polymer–matrix composites, studies based on CNT composites have been broadly conducted; most of these have focused on the dispersion and modification of CNTs[36–42] or changes in the curing kinetics and mechanical, thermal, and electric properties caused by the addition of different amounts of CNTs in

the terrestrial environment.[43–51] However, there have been few studies concentrating on the curing process of CNT composites under microgravity or on the properties of CNT composites cured in different gravity environments. Because of the various applications of CNT composites in aerospace, it is significant to conduct related experiments in simulated space environments on the ground, such as the microgravity environment, where there is no sedimentation or convection, to promote the potential applications of CNT composites and other resin matrix materials.

The microgravity environment has been obtained mainly by free fall (drop tubes, drop towers), parabolic flight, and space station experiments, with their limitations of achieving a microgravity of less than 30 seconds, expensive equipment, or complex procedures.[52] Some other methods, including rotary cell culture systems and random positioning machines[53,54] have been used for the simulation of microgravity, with the requirement of liquid conditions or/and small sizes. Hence, other simple and cost-effective methods for the simulation of microgravity still needed to be explored. A superconducting magnet (JASTEC-16T) with an ultrastrong magnetic force produced by a superconducting coil was used to simulate different gravity environments in this study; this was cost effective and could last for a long time, even years. The feasibility of this equipment has been verified, on the basis of which some studies in life sciences and materials sciences have been conducted.[55–57]

In this study, we investigated the influences of simulated microgravity environments on the curing process of the amino-functionalized multiwalled carbon nanotube (NH_2-MWCNT)-reinforced epoxy E51 (0.5 wt % NH_2-MWCNTs). Fourier transform infrared (FTIR) spectroscopy and differential scanning calorimetry (DSC) were conducted to characterize the effects. Meanwhile, the performances of the different systems cured in the three different gravity environments simulated on the ground were explored with dynamic mechanical analysis (DMA), thermomechanical analysis (TMA), thermogravimetric analysis (TGA), scanning electronic microscopy (SEM), transmission electron microscopy (TEM), and three-point bending tests. The results show that in the simulated microgravity environment, the curing rate and α decreased. The performances of the upper and lower parts of the same sample, as demonstrated by the α, storage modulus (E'), linear expansion coefficient, and bending stress, were relatively close to each other and had better uniformity compared to those in the terrestrial gravity environment. Through detailed experiments, many new phenomena were obtained and analyzed.

EXPERIMENTAL

Materials

The epoxy resin used in the experiments was bisphenol A glycidyl ether epoxy resin E51; it was purchased from Wuxi Resin Factory of Bluestar New Chemical Materials Co., Ltd. (Jiangsu, China) with an epoxy value of 0.5 ± 0.01 (epoxy equivalent weight = 184–195 g/equiv, degree of polymerization in the chemical structure = 0.18–0.24).

The curing agent was a modified amine (named 593) purchased from Shanghai Resin Factory Co., Ltd. (Shanghai, China).

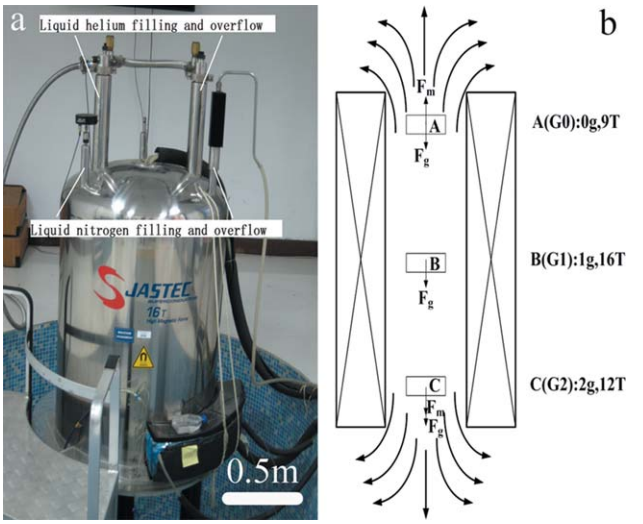

Figure 1. (a) Photo of the superconducting magnet with a scale bar of 0.5 m. (b) Positions and magnetic field intensity of the different gravity areas simulated by the superconducting magnet, where F_g means gravity and F_m means magnetic force. [Color figure can be viewed in the online issue, which is available at wileyonlinelibrary.com.]

It was a transparent liquid and had long-chain structures; its viscosity was 80–100 mPa.s (298.15 K).

NH_2-MWCNTs were purchased from Chengdu Organic Chemicals Co., Ltd., Chinese Academy of Sciences (Chengdu, China, average length = 50 μm, diameter = 8–15 nm, —NH_2 content = 0.45 wt %, and purity > 95 wt %.

Simulation Equipment

The superconducting magnet simulated three different gravity environments at the same time as is shown in Figure 1; the three areas corresponded to different magnetic field strengths (9T, 16T, and 12T), including simulated 0, 1, and 2 g, respectively. The contrast gravity environment was terrestrial (1 g); this corresponded to (0.5×10^{-4})T. The four gravity environments, including terrestrial 1 g and simulated 0, 1, and 2 g were abbreviated as G, G0, G1, and G2, respectively, in the following text.

Sample Preparation

In this study, we selected a direct method in which the NH_2-MWCNTs were added to the resin directly with mass fractions of 0.1, 0.3, 0.5, and 1 wt % according to the previous reports on CNT composites.[36,48,58] The preparation of the NH_2-MWCNT-reinforced epoxy composites was done as follows:

The resin was heated to 70°C; this was followed by the addition of certain mass fractions of NH_2-MWCNTs into the resin with a continuous stirring. Then, the mixture was cooled to room temperature after it was dispersed by ultrasonic vibration for 2 h. A certain proportion of the curing agent (E51:593 = 1:0.2768) was added to the mixture; this was followed by degassing with a vacuum pump for about 5 min. Then, the mixture was poured into aluminum molds, which were put into the four gravity environments, G, G0, G1, and G2, with an environmental temperature of 40°C.

The study of the curing process was carried out on basis of the composite with 0.5 wt % NH_2-MWCNTs cured in the G and

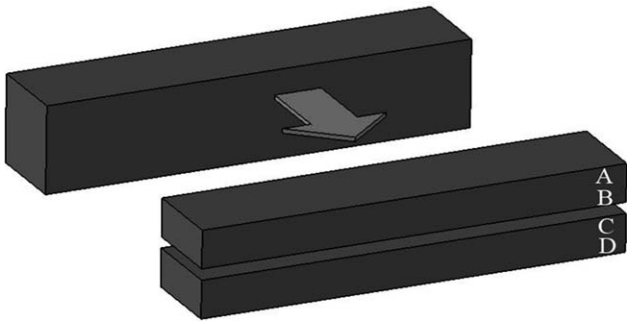

Figure 2. Scheme of the cutting method.

G0 environments. The method for sample collection was based on previous experiments,[59] in which samples were collected according to different curing times corresponding to the different αs. In this study, the specimens with an α of 0% were collected immediately after the mixture was stirred evenly. Specimens with αs of 20, 40, 60, 80, and 90% were collected at the same location of the samples cured in the G and G0 environments according to the corresponding time. The collected specimens were put into 1.5-mL sample tubes, and the tubes were sealed with a seal membrane and hanged in a liquid nitrogen tank to wait for the DSC and FTIR tests.

When we studied the properties of the cured products, the samples obtained after the mixture were put into the environments for 4 h. To explore the influences of different gravities on the properties of the different parts of one sample, each sample was cut into upper and lower parts to compare their properties. The cutting method is shown in Figure 2.

The testing results were named as *X-nm,* where *X* indicates different gravity values, including G, G0, G1, and G2; *n* indicates different collection times of the specimens (with 1 to 6 indicating 15, 30, 50, 70, 90, and 240 min, respectively); and *m* indicates the location of the specimen collection, including the upper part (U) and the lower part (D). According to this naming principle, G-1U indicates that the specimen was cured in a terrestrial gravitation environment and collected at the specified upper part after 15 min of curing.

Characterizations

FTIR spectroscopy was carried out with an Equinox 55 FTIR spectrometer (Bruker, Germany) in the wavelength range 4000–400 cm^{-1} at a resolution of 4 cm^{-1}.

DSC was carried out with a STARe system analyzer (Mettler-Toledo, Switzerland) with samples heated up from 20 to 200°C at a heating rate of 10°C/min under a nitrogen atmosphere.

The E' and tan δ values were tested with DMA (SDTA861e, Mettler-Toledo). The measurements were taken under a shear mode over a temperature range from 25 to 145°C at a heating rate of 5°C/min with a frequency of 1 Hz, an amplitude of 3 μm, a force of 5 N, and the sample size of 10 × 3.4 mm^2.

TGA was carried out in TGA/DSC STARe system (Mettler-Toledo) with a heating rate of 10°C/min from 30 to 700°C under a nitrogen atmosphere.

The coefficient of thermal expansion (CTE) was measured with a TMA/SDTA840 (Mettler-Toledo) at a heating rate of 5°C/min from room temperature to 250°C with a sample size of 10 × 3.4 mm^2.

A three-point bending test was conducted with an Instron 5965 universal material tester (Instron) at room temperature with a crosshead speed of 2 mm/min. We obtained all of the data by testing samples for three times with a sample size of 35 × 7 × 3.4 mm^3.

SEM images of the fracture surfaces were obtained with a Helios Nanolab600i electronic microscope (FEI). The specimen surfaces were coated with a thin gold film to increase their conductance for SEM observation. The area of the gold-coated surfaces was an average of 7 × 3.4 mm^2.

TEM images were obtained by a Hitachi-7650 (Hitachi, Japan). The cured samples were cut into 70–90 nm with a diamond knife of the ultramicrotome; the cut sections were then transferred to a copper TEM grid and examined under TEM at an acceleration voltage of 100 kV.

RESULTS AND DISCUSSION

Characterizations of the Curing Process in Different Gravity Environments

FTIR Spectroscopy. It is well known that the reaction of E51, the NH_2-MWCNTs, and the curing agent 593 was based on the reaction of amino groups and epoxy groups. Because of the constant change of primary amines, secondary amines, and tertiary amines during the curing process, the curing process was monitored mainly by means of observations of the changes in the epoxy group absorption peak. In the fingerprint region, the epoxy group had three characteristic peaks: 830, 913, and 1250 cm^{-1}. The absorption peak hardly changed at 830 cm^{-1} and was overlapped with the bending vibrations of two adjacent hydrogen atoms of the benzene ring with paraorientation.[26] So, in this study, the curing speed of the samples in different gravity environments was analyzed through the calculation of the peak area ratio of the epoxy group (at 913 cm^{-1}) to benzene ring (1594 cm^{-1}) in the IR spectrogram.

After the calculation, we found that the upper-part curing speeds of the samples in G were all higher than those in G0 from the first to fifth collecting stage. In the sixth stage (as is shown in Figure 3), we calculated the peak area ratio of the epoxy group to the benzene ring of the upper and lower part of the samples; these were 0.2131(U) and 0.2049(D) in G and 0.1916(U) and 0.1807(D) in G0, respectively. The calculation results show that the curing speed of the epoxy materials in G were higher than those in G0, but the homogeneity of the materials in G was worse than that in the materials cured in G0. Furthermore, there was a small absorption peak of the epoxy group existing in every IR spectrogram because of a lack of postcuring at higher temperatures.

DSC. Both the NH_2-MWCNTs and the curing agent 593 could react with the epoxy resin so there should have been two peaks appearing in the curing exothermic curve. However, as is shown in Figure 4, there was only one main exothermic peak in the curve of the 0.5 wt % NH_2-MWCNT-reinforced epoxy; its

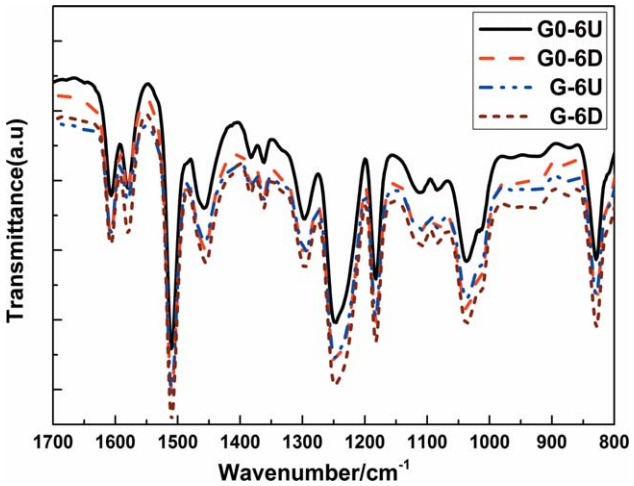

Figure 3. FTIR spectra of the upper and lower parts of the sample collected in the sixth stage. [Color figure can be viewed in the online issue, which is available at wileyonlinelibrary.com.]

appearance did not change obviously compared to that of E51. There were two possible reasons for this phenomenon: one was that the released heat of the reaction between the NH_2-MWCNTs and the epoxy resin was too low to be observed compared to that of the reaction between the curing agent 593 and the epoxy resin. The other reason was that the reaction between the NH_2-MWCNTs and the epoxy resin completed during the dispersion process by ultrasonication; this might have been the main reason. According to eq. (1), the αs were calculated through the released heat, as shown in Figure 5:

$$\alpha = 1 - H_t / H_0 \quad (1)$$

where H_0 is the total heat of the reaction and H_t is the residual heat at time t.

As shown in Figure 5, the α values of the specimens increased with increasing curing time. The growth speed was fast before the third stage and then became slow between the third and fifth stage. After the fifth stage, it reached a plateau. At the sixth stage, the α reached approximately 100%. This phenomenon could be explained as follows: in the first segment of the curing reaction, the first and second stage, the systems were in a liquid or rubbery state. The micromolecules could be polymerized into macromolecular chains easily, so α increased rapidly in this segment. In the second segment, the reaction systems reached a gel state, and the viscosity of the reaction system became larger; this limited the movement of molecular segments and postponed the curing reaction. However, the curing reaction still proceeded slowly with increasing curing time in this segment; this could be explained the slow growth of α from the third to fifth stage. When the curing reaction reached the sixth stage, the movement of molecular segments was almost stopped, and the systems had already formed the three-dimensional network structure. In this stage, the improvement of α required a higher curing temperature rather than a longer curing time.

Compared to the α of specimens in the G and G0 environments, it was clear that the αs of every stage in G–nU were all slightly higher than those in G0–nU. At the sixth stage, we obtained two conclusions: (1) the α of the lower part was slightly higher than that of the upper part of the same sample and (2) the α of the upper and lower part of the same sample in G0 was closer than that in G; that is, the samples cured in G0 were more uniform than those cured in G.

The prepared mixture with the epoxy and curing agent was uniform [as shown in Figure 6(a)]; this was influenced by different gravity environments. In G, the macromolecular chains and gels produced in the curing reaction sank down because of the gravity [as is shown in Figure 6(b)]; this was the sedimentation phenomenon. This sinking behavior made the exothermic macromolecule chains and gels gather at the lower part of the samples and led to heat concentration at the lower part of one sample, as is shown in Figure 6(c). According to the characteristics of the catalytic reaction, the heat concentration accelerated

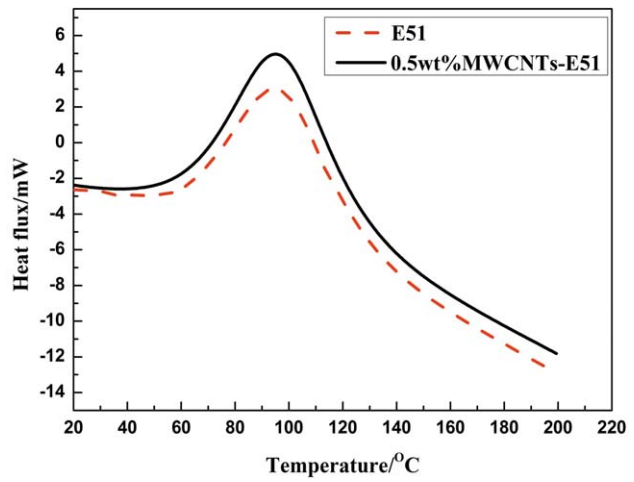

Figure 4. Curing exothermic curves of E51 and 0.5 wt % NH_2-MWCNTs reinforced E51 in G (MWCNT = multiwalled carbon nanotube). [Color figure can be viewed in the online issue, which is available at wileyonlinelibrary.com.]

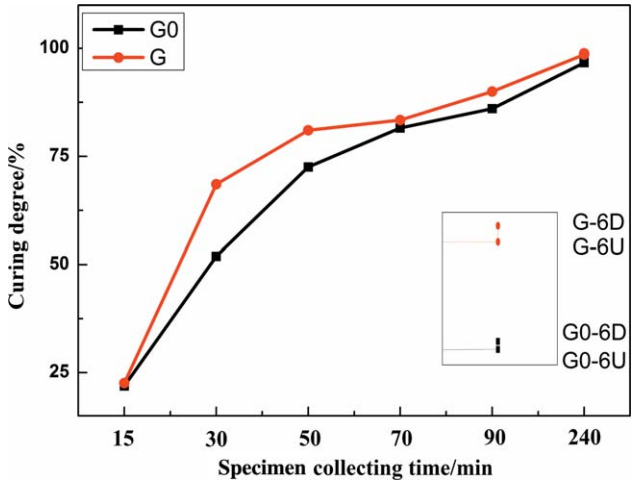

Figure 5. αs of 0.5 wt % NH_2-MWCNT-reinforced E51 cured in the G and G0 environments with different specimen collection times; the inset image shows the αs of the upper and lower parts of the sample collected in the sixth stage. [Color figure can be viewed in the online issue, which is available at wileyonlinelibrary.com.]

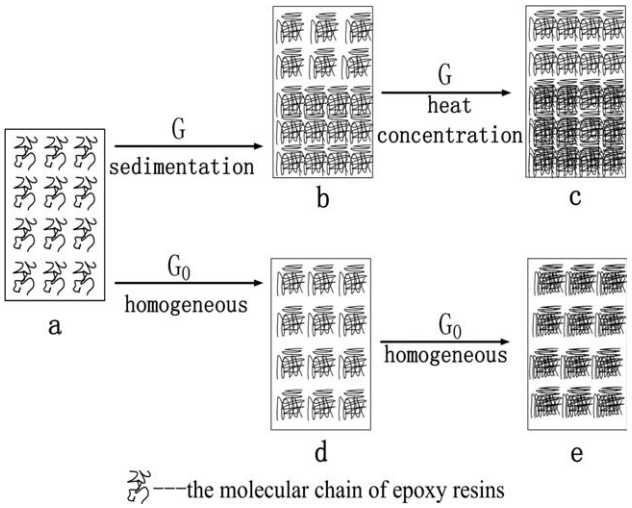

Figure 6. Schematic diagram of the different curing processes in the G and G0 environments.

the reaction in this area and generated more heat; this made the whole sample cure at a higher ambient temperature. In G0, the sedimentation phenomenon disappeared, and each part of the sample had uniform heat, as shown in Figure 6(d); this weakened the effects of the catalytic reaction. Hence, the curing speed in G0 became slower than that in G. The whole sample was finally cured in a lower ambient temperature, as shown in Figure 6(e).

As shown by the previous analysis, the α of a sample cured in G was higher than that of the material cured in G0. In the sixth stage, although the difference between the αs in the upper and lower parts of the same sample became less obvious in G0 than that in G, it still existed in G0 environment. There were two probable reasons: (1) the parameters in G0 could not reach the theoretical values completely, which could not thoroughly eliminate the effect of the sedimentation and (2) the existing superstrong magnetic field might have interfered with the effects of the simulated microgravity or the curing reaction.[55]

Characterizations of the Resin Systems Cured in Different Gravity Environments

DMA. The load-bearing capacity of a composite can be determined by its dynamic E'. As is shown in Figure 7(a), the values of log E' of the pure epoxy cured in G below the glass-transition region were higher than those of the material cured in the G0 environment. The difference of the log E' between the upper and lower parts of the specimens cured in G0 was less obvious than the samples cured in the G environment. As mentioned previously, in the G environment, the whole sample was cured at a higher ambient temperature and got a higher α because of the heat concentration caused by sedimentation, but in the G0 environment, the whole sample was cured at a lower ambient temperature and got a lower α. The movement of the molecular segments was hindered because of the high α. This led to the higher E' in G below the glass-transition region.

As shown in Figure 7(b), the difference between the E' values of the upper and lower part of one sample cured in G0 was less obvious than that of the material cured in the G environment. This was consistent with the DSC results. Compared to pure epoxy, the E' of the composite increased with the amount of NH_2-MWCNTs added to the systems; this could be explained by the reinforcement effects of the NH_2-MWCNTs to the stiffness of composite.[31,60] When the NH_2-MWCNTs were added to the systems before the curing agent 593 was added, their amine groups had more chances and time to react with the epoxy groups of E51; this led to the ring-opening reaction and the formation of covalent bonds between the amine groups and epoxy groups. The reaction improved the crosslinking density of the epoxy composites and promoted the formation of the crosslinked structure, which restricted the movement of molecular chains linked with the NH_2-MWCNTs and increased the E' of the composite.[32]

As shown in Figure 7, we also found that there were obvious differences in the E' values in the glassy region for the tested systems rather in contrast to the rubbery region. This occurred because of the higher molecular motion after the glass-transition region. This was explained in a previous report;[61] that is, the molecular motion remained high, and there was no

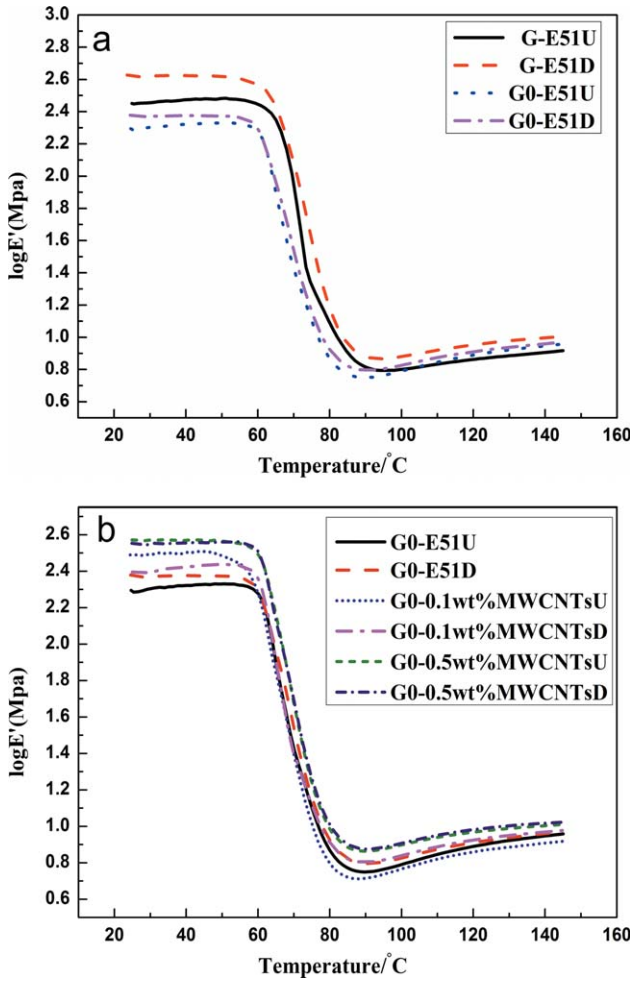

Figure 7. Log E' of (a) E51 cured in different environments and (b) different systems cured in the G0 environment (MWCNT = multiwalled carbon nanotube). [Color figure can be viewed in the online issue, which is available at wileyonlinelibrary.com.]

shear force between the macromolecules in the rubbery state. At the end of the rubbery region, the E' values of every specimen showed a slight growth trend, which was due to the absence of postcuring at higher temperatures.

The ratio of the loss modulus to E' was measured as tan δ. The relaxation peak of the tan δ curve was ascribed to the glass-transition temperature (T_g), and the height of the tan δ peak was associated with the crosslink density. The lower crosslink density resulted in a higher segmental mobility and higher peak height at T_g.

Because of the different αs caused by the heat concentration, the T_g and relaxation peak height values of the pure epoxy cured in the G0 environment were all slightly lower than those of the material cured in the G environment, as shown in Figure 8(a). From Figure 8(b), we observed that the T_g values of the three systems cured in the G0 environment showed no obvious changes. However, the peak heights became lower with the addition of the NH_2-MWCNTs; this was because the uniform distribution of NH_2-MWCNTs might have hindered the mobility of the epoxy main chains linked with them by interfacial

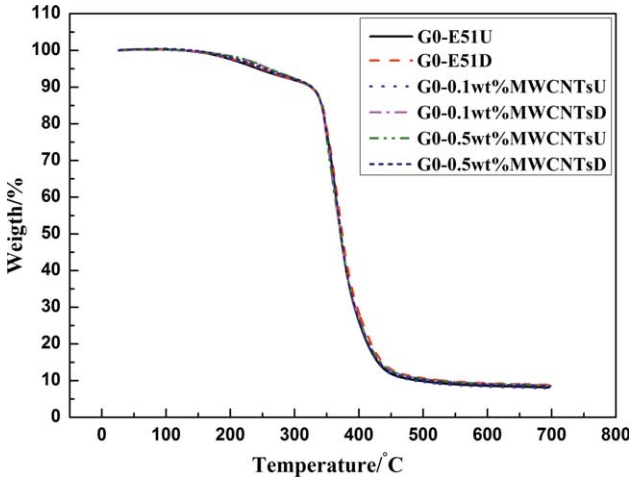

Figure 9. TGA thermograms of E51 and 0.1 and 0.5 wt % NH_2-MWCNTs cured in the G0 environment (MWCNT = multiwalled carbon nanotube). [Color figure can be viewed in the online issue, which is available at wileyonlinelibrary.com.]

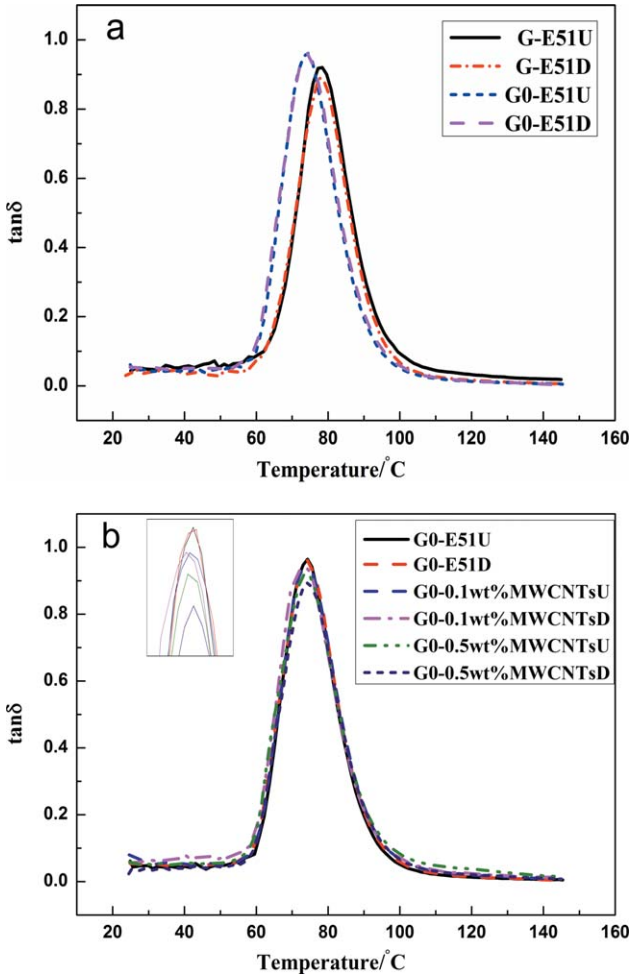

Figure 8. Tan δ of (a) E51 cured in different environments and (b) different systems cured in the G0 environment (MWCNT = multiwalled carbon nanotube). [Color figure can be viewed in the online issue, which is available at wileyonlinelibrary.com.]

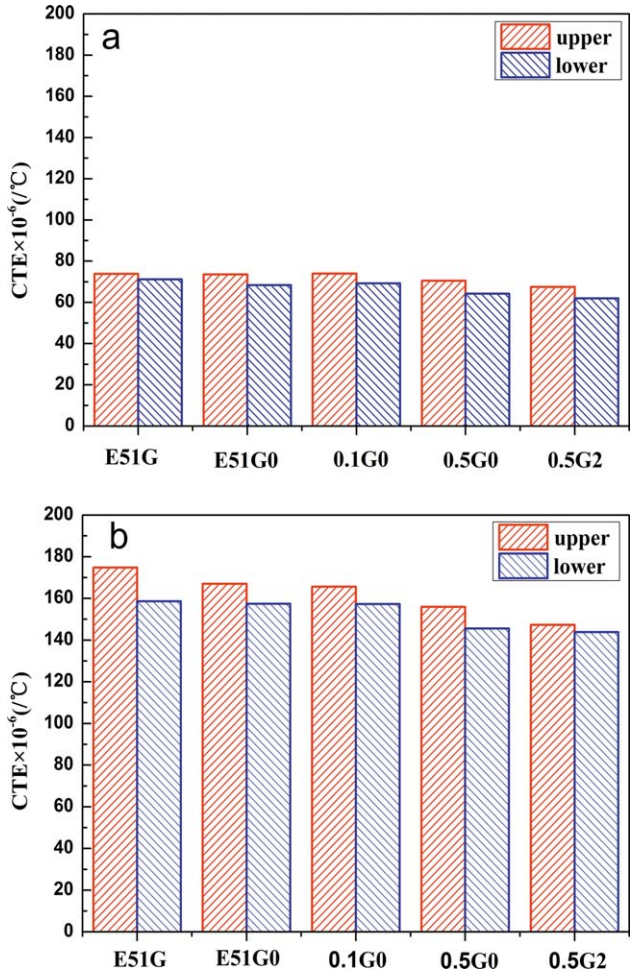

Figure 10. CTEs of different systems cured in different gravity environments, (a) before T_g and (b) after T_g. [Color figure can be viewed in the online issue, which is available at wileyonlinelibrary.com.]

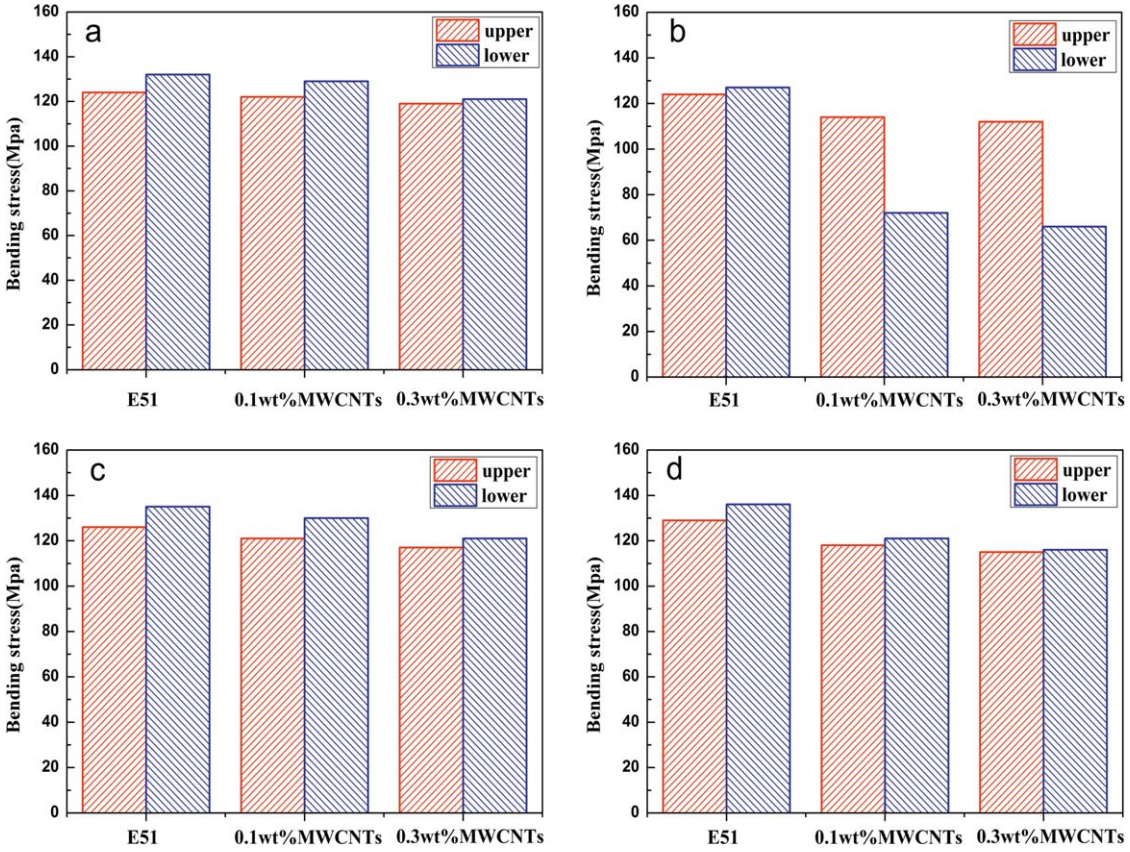

Figure 11. Bending stress of different parts of the specimens cured in the G and G0 environments tested under different force directions: (a) G, upper (B–A) and lower (C–D); (b) G0, upper (B–A) and lower (C–D); (c) G, upper (B–A) and lower (D–C); and (d) G0, upper (B–A) and lower (D–C). MWCNT = multiwalled carbon nanotube. [Color figure can be viewed in the online issue, which is available at wileyonlinelibrary.com.]

interaction. This led to a decrease in the motion amplitude of the molecular chain segments.

TGA. The thermal stability of different samples cured in the G0 environment was studied by TGA in a nitrogen atmosphere (Figure 9). The thermal stability could be expressed in terms of parameters such as the initial decomposition temperature, maximum rate of degradation temperature, and final residue rate, but as shown in Figure 9, it was obvious that the TGA curves of the different specimens and different parts of the same sample were all the same. The curves in Figure 9 indicate that the thermal stability of the pure epoxy resin in a nitrogen atmosphere were not affected by the small addition of NH_2-MWCNTs, and the same conclusion was obtained for the different parts of the same sample.

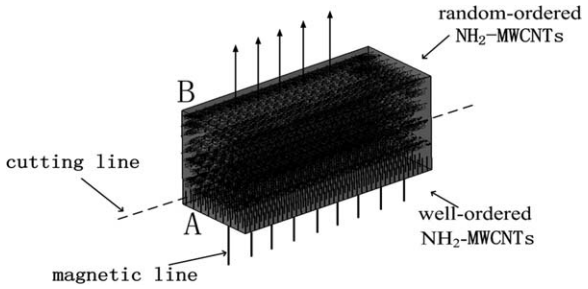

Figure 12. Schematic diagram of the NH_2-MWCNTs dispersed in the composite under a strong magnetic field.

CTE. The influences of the different gravity environments and addition amounts of NH_2-MWCNTs on the thermal expansion of the composite were analyzed through a comparison of the CTE values of different specimens. The comparison between G-E51 and G0-E51 showed the influence of the microgravity environment on the thermal expansion of the pure epoxy system (E51G and E51G0 in Figure 10). The comparison among G0-E51, G0-0.1 wt %, and G0-0.5 wt % NH_2-MWCNTs illustrated the influences of different addition amounts of NH_2-MWCNTs on the thermal expansion (E51G0, 0.1G0, and 0.5G0 in Figure 10). To magnify the influences of gravity, the G0-0.5 wt % and G2-0.5 wt % NH_2-MWCNT systems were also compared (0.5G0 and 0.5G2 in Figure 10). It was clear that the dimensional change of every sample increased with the growth of temperature. To quantify the comparison, the CTE was calculated by eq. (2):[32]

$$\alpha=(1/L_0)(\Delta L/\Delta T) \quad (2)$$

where L_0 is the initial dimension, ΔL is the change in the length, and ΔT is the change in the temperature.

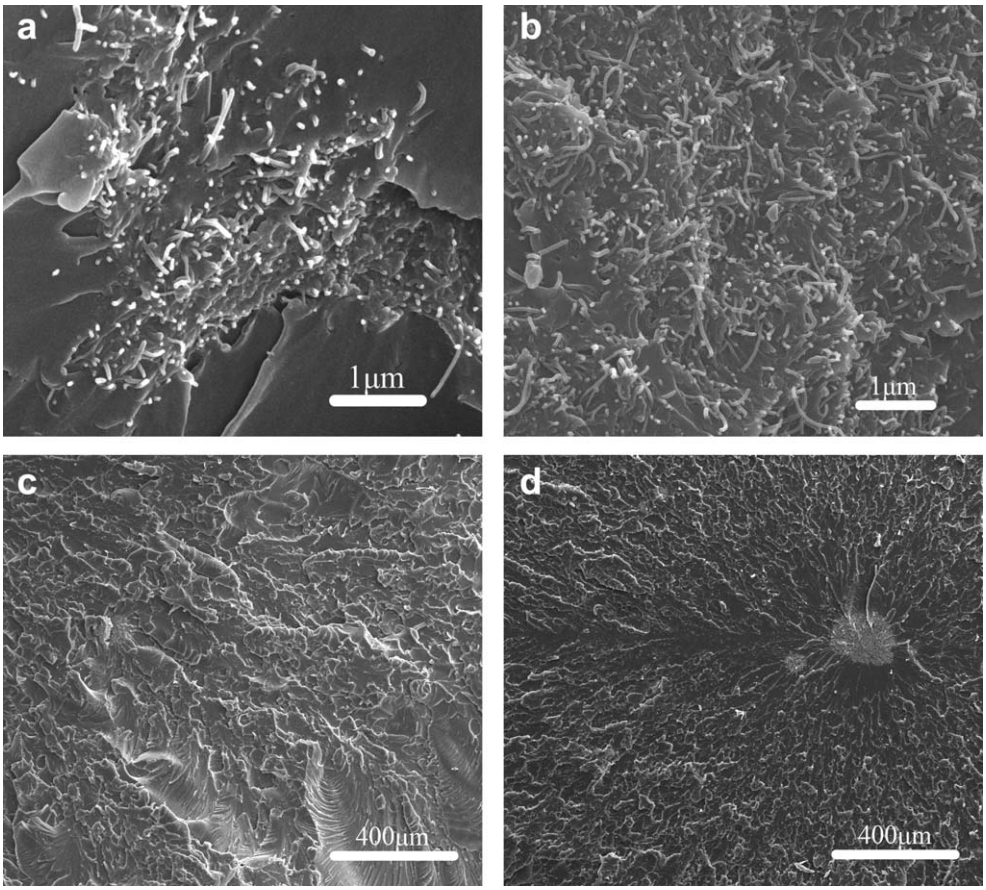

Figure 13. SEM images of (a) NH_2-MWCNTs well-ordered in the entrance of magnetic line and were pulled out of the matrix, (b) NH_2-MWCNTs randomly ordered in the exit of magnetic line, (c) ductile fracture, and (d) severe aggregation of the NH_2-MWCNTs.

The values of CTE below and above the T_g of the pure epoxy and composite with NH_2-MWCNTs are shown in Figure 10.

The CTE value is directly related to the free volume properties of resin systems, which is determined by the crosslinking density.[62] When the curing temperature is higher, the crosslinking density is bigger, but the free volume is smaller. As is shown in Figure 10, the CTE values of the same specimen after T_g were all higher than those before T_g; this resulted from the molecular interaction. With increasing temperature, the molecular vibration in the material increased; this caused an increase in the intermolecular distance.[1] As shown in Figure 10, the CTE value of the upper part was lower than that of the lower part of the same sample because of the different abilities of molecular movement in different areas with different αs. When we compared the CTE values of the pure epoxy and composite with those of the NH_2-MWCNTs, we found that the values became lower with the addition of NH_2-MWCNTs because of the lower CTE value of the NH_2-MWCNTs. Meanwhile, the NH_2-MWCNTs reduced the motion of the macromolecular segments around them and improved the interfacial adhesion between them and the epoxy matrix.

Three-Point Bending Testing. With the cutting way shown in Figure 2, the force direction of the upper part was B–A stationary, and the direction of the lower part was C–D [the results are shown in Figure 11(a,b)] and D–C [the results are shown in Figure 11(c,d)]. The bending stress of the specimens declined slightly with the addition of NH_2-MWCNTs; this might have been due to the agglomeration caused by the inappropriate dispersion method or the length of the NH_2-MWCNTs. The bending stress of the lower part of one sample before and after the change in the force direction changed inconspicuously in G [as is shown in Figure 11(a,c)], but it changed tremendously in G0 [as is shown in Figure11(b,d)]. We concluded that composites with NH_2-MWCNTs cured in a strong magnetic field exhibited a higher bending stress when the force direction was along with the direction of the magnetic field lines. To explain the previous conclusion, a conjecture was proposed: as in the previous statement, the magnetic field strength of superconducting magnet environment was six orders of magnitude higher than that of the terrestrial environment; this could have led to the deflection of the magnetic moment of the substances in the magnetic field. Because of the combination of the strong magnetic field and the microscale effect of the NH_2-MWCNTs, there was a deflection of the dispersed NH_2-MWCNTs with their magnetic moment in the strong magnetic field. This resulted in a well-ordered distribution of NH_2-MWCNTs in the composite. Because there might have been an attenuation of the magnetic field strength with the magnetic force through the composite, it was possible that the NH_2-MWCNTs became well ordered in

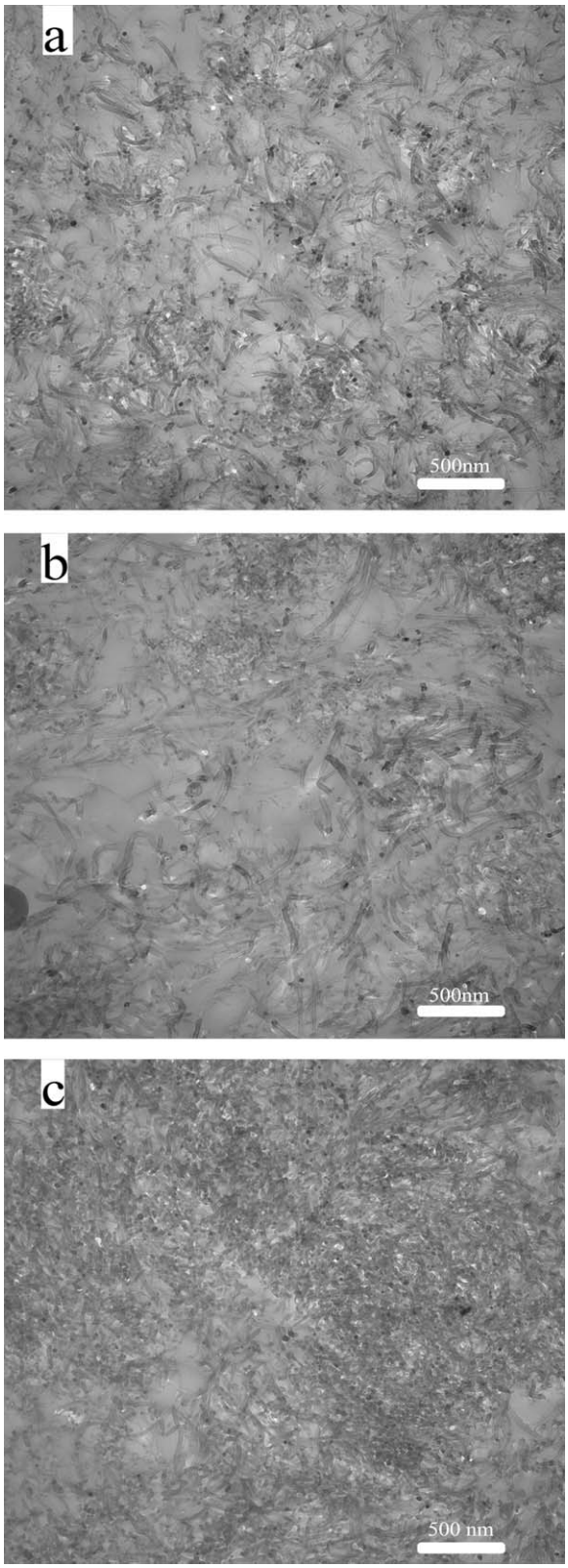

Figure 14. TEM photographs of the 0.5 wt % NH_2-MWCNTs dispersion in the (a) G, (b) G0, and (c) G2 environments.

the entrance side of the magnetic line (side A in Figure 12) but randomly ordered in the other side (side B in Figure 12) with the influence of the change in the composite concentration. To observe the possible different array of NH_2-MWCNTs in the contrary side of one sample, the SEM images of the corresponding side were taken and are shown in Figure 13(a,b). The array of the NH_2-MWCNTs was well-ordered in Figure 13(a) and randomly ordered in Figure 13(b); these images were consistent with the schematic diagram of Figure 12.

SEM. The interfacial reaction between amine groups of the NH_2-MWCNTs and the epoxy groups of E51 resulted in the ring-opening reaction and the formation of a crosslinked structure, which produced a strong combination between the NH_2-MWCNTs and the epoxy matrix. Meanwhile, with the characteristics of a high aspect ratio and high strength, the NH_2-MWCNTs could be pulled out of the matrix rather than broken immediately during crack propagation in the matrix [as shown in Figure 13(a)]. During this process, the energy of the crack tips decreased dramatically or were forced to arrest; this resulted in a change in the crack propagation. Along with the crack propagation, the sample was fractured, and the fractograph exhibited a typical ductile dimple fracture pattern [as shown in Figure 13(c)]. If the addition amount of NH_2-MWCNTs was excessive, the mechanical properties of the composites subsided. Just as in the experiments done in this study, there was severe agglomeration with the addition amount of 0.5 wt % NH_2-MWCNTs [as is shown in Figure 13(d)]. If the addition amount increased to 1 wt % or more, the composites were attached with more defects, such as bubbles, when they were cured with the same curing method.

TEM. To compare the dispersion of NH_2-MWCNTs in the G, G0, and G2 environments, an NH_2-MWCNT addition amount of 0.5 wt % was selected for the TEM test. As shown in Figure 14, the NH_2-MWCNTs dispersed in the three samples were all randomly ordered; this was probably because the magnetic field could not make all of the NH_2-MWCNTs have a well-ordered dispersion but only a small amount (as shown in Figure 12) could achieve this because of the attenuation of the magnetic field intensity or the resistance of the resin matrix. Furthermore, the well-ordered NH_2-MWCNTs could not be found in Figure 14; this might have been due to the slicing way for the TEM test. When the three images in Figure 14 were compared, it was clear that the quantity of NH_2-MWCNTs in the lower part of the sample cured in the G2 environment was greater than that in the other two environments, and this proved the influence of gravity.

CONCLUSIONS

In this study, we investigated the influences of different gravity values on the curing process and performances of resin matrix composites with NH_2-MWCNTs. Several conclusions are listed as follows:

1. The curing process and production performances of the resin matrix composites with NH_2-MWCNTs were obviously influenced by the gravity effect. In the terrestrial gravity environment, the heat concentration caused by sedimentation promoted the curing reaction and made the systems cure at a relatively high ambient temperature. This made the cured products have a higher α than those with no heat concentration. However, in the microgravity environment,

there was no heat concentration, and the system was in a homogeneous environment, in which the cured products became more homogeneous than those cured in the gravity environment.
2. T_g and the thermal stability of the resin matrix composites were not be influenced by the addition of a small amount (0.1–0.5 wt %) of NH_2-MWCNTs when the composites were cured in a microgravity environment.
3. The CTE values of the tested samples after T_g were all higher than those before T_g. For each sample, the CTE value of the upper part was bigger than that of the lower part. After the addition of NH_2-MWCNTs into the resin matrix composites, the CTE values decreased, and the differences between the upper and lower part of the same sample became less obvious.
4. The NH_2-MWCNTs combined well with the resin matrix because of the reaction between amine groups and epoxy groups. The bending stress of the NH_2-MWCNT-reinforced composite cured in a microgravity environment simulated by a superconducting magnet changed dramatically when the composites were tested under opposite force.

ACKNOWLEDGMENTS

This work was financially supported by the Fundamental Research Funds for the Central Universities (contract grant number HIT.-KISTP.201408), the Program for Harbin City Science and Technology Innovation Talents of Special Fund Project (contract grant number 2012RFXXG091), and the Pre-Research Fund Project of National Defense.

REFERENCES

1. Jyotishkumar, P.; Abraham, E.; George, S. M.; Elias, E.; Pionteck, J.; Moldenaers, P.; Thomas, S. *J. Appl. Polym. Sci.* **2013**, *10*, 3093.
2. Wang, L.; Liu, D. Q.; Wang, X. J.; Han, X. *J. Chem. Eng. Sci.* **2012**, *81*, 157.
3. Jyotishkumar, P.; Pionteck, J.; Özdilek, C.; Moldenaers, P.; Cvelbar, U.; Mozetic, M.; Thomas, S. *Soft Matter* **2011**, *7*, 7248.
4. Im, J. S.; Jeong, E.; In, S. J.; Lee, Y. *Compos. Sci. Technol.* **2010**, *70*, 763.
5. Tsang, C. F.; Hui, H. K. *Thermochim. Acta* **2001**, *367–368*, 93.
6. Park, S. J.; Jin, F. L. *Polym. Degrad. Stab.* **2004**, *86*, 515.
7. Iqbala, K.; Khana, S.; Munirb, A.; Kim, J. *Compos. Sci. Technol.* **2009**, *69*, 1949.
8. Kang, S. K.; Lee, D. B.; Choi, N. S. *Compos. Sci. Technol.* **2009**, *69*, 245.
9. Yang, T.; Zhang, C. F.; Zhang, J.; Cheng, Y. *J. Thermochim. Acta* **2014**, *577*, 11.
10. Kim, W. G.; Lee, J. Y. *Polymer* **2002**, *43*, 5713.
11. Vinnik, R. M.; Roznyatovsky, V. A. *J. Therm. Anal. Calorim.* **2003**, *73*, 807.
12. Vyazovkin, S. *Anal. Chem.* **2006**, *78*, 3875.
13. Merline, J. D.; Nair, C. P. R.; Gouri, C.; Sadhana, R.; Ninan, K. N. *Eur. Polym.* **2007**, *43*, 3629.
14. Sun, H.; Liu, Y. Y.; Tan, H. F.; Du, X. W. *Appl. Polym. Sci.* **2014**, *39882*, 1.
15. Lavorgna, M.; Romeo, V.; Martone, A.; Zarrelli, M.; Giordano, M.; Buonocore, G. G.; Qu, M. Z.; Fei, G. X.; Xia, H. S. *Eur. Polym. J.* **2013**, *49*, 428.
16. Yu, H. O.; Liu, J.; Wen, X.; Jiang, Z. W.; Wang, Y. J.; Wang, L.; Zheng, J.; Fu, S. Y.; Tang, T. *Polymer* **2011**, *52*, 4891.
17. Palmeri, M. J.; Putz, K. W.; Ramanathan, T.; Brinson, L. C. *Compos. Sci. Technol.* **2011**, *71*, 79.
18. Bakar, M.; Kostrzewa, M. J. *Thermoplast. Compos. Mater.* **2010**, *23*, 749.
19. Guan, J. W.; Ashrai, B.; Martinez-Rubi, Y.; Zhang, Y.; Kingston, C. T.; Johnston, A.; Simard, B. *Polym. Polym. Compos.* **2011**, *19*, 99.
20. Kondyurin, A. *Adv. Space Res.* **2001**, *28*, 665.
21. Kondyurin, A.; Lauke, B.; Kondyurina, I.; Orba, E. *Adv. Space Res.* **2004**, *34*, 1585.
22. Briskman, V.; Kostarev, K.; Yudina, T.; Levtov, V.; Romanov, V. AIAA 95, **1995**, 0263.
23. Briskman, V.; Kostarev, K.; Levtov, V.; Lyubimova, T.; Mshinsky, A.; Nechitailo, G.; Romanov, V. *Acta Astronautica* **1996**, *39*, 395.
24. Briskman, V. A. *Adv. Space Res.* **1999**, *24*, 1199.
25. Sorrentino, L.; Tersigni, L. *Appl. Compos. Mater.* **2012**, *19*, 31.
26. Yang, K.; Gu, M. Y.; Jin, Y. P. *J. Appl. Polym. Sci.* **2008**, *110*, 2980.
27. Chen, Q.; Xu, R. W.; Yu, D. S. *Polymer* **2006**, *47*, 7711.
28. Gojny, F. H.; Schulte, K. *Compos. Sci. Technol.* **2004**, *64*, 2303.
29. Bai, J. B.; Allaoui, A. *Compos. A* **2003**, *34*, 689.
30. Gojny, F. H.; Wichmann, M. H. G.; Fiedler, B.; Kinlochb, I. A.; Bauhoferc, W.; Windleb, A. H.; Schultea, K. *Polymer* **2006**, *47*, 2036.
31. Wang, Y. T.; Wang, C. S.; Yin, H. Y.; Wang, L. L.; Xie, H. F.; Cheng, R. S. *Express Polym. Lett.* **2012**, *6*, 719.
32. Rahman, M. M.; Hosur, M.; Ludwick, A. G.; Zainuddin, S.; Kumar, A.; Trovillion, J.; Jeelani, S. *Polym. Test.* **2012**, *31*, 777.
33. Berketis, K.; Tzetzis, D. *J. Mater. Sci.* **2009**, *44*, 3578.
34. Ramirez, F. A.; Carlsson, L. A.; Acha, B. A. *J. Mater. Sci.* **2008**, *43*, 5230.
35. Atas, C.; Sayman, O. *Compos. Struct.* **2008**, *82*, 336.
36. Jagtap, S. B.; Ratna, D. *Express Polym. Lett.* **2013**, *7*, 329.
37. Yi, X. F.; Mishra, A. K.; Kim, N. H.; Ku, B. C.; Lee, J. H. *Compos. A* **2013**, *49*, 58.
38. Gojny, F. H.; Nastalczyk, J.; Roslaniec, Z.; Schulte, K. *Chem. Phys. Lett.* **2003**, *370*, 820.
39. Damian, C. M.; Pandele, A. M.; Andronescu, C.; Ghebaura, A.; Gareaa, S. A.; Iovua, H. *Fullerenes, Nanotubes Carbon Nanostruct.* **2011**, *19*, 197.

40. Chen, H.; Wang, C. C.; Chen, C. Y. *Plasma Proc. Polym.* **2010**, *7*, 59.
41. Maria, W. P.; Wesolek, D.; Gieparda, W.; Ska, A. B.; Ciecierska, E. *Polym. Adv. Technol.* **2011**, *22*, 48.
42. Deng, H.; Cao, Q.; Wang, X.; Chen, Q.; Kuang, H.; Wang, X. F. *Mater. Sci. Eng. A* **2011**, *528*, 5759.
43. Zhang, A. B.; Liu, W.; Li, M.; Zheng, Y. P. *J. Reinf. Plast. Compos.* **2009**, *28*, 2405.
44. Przybylak, M. W.; Wesolek, D.; Gieparda, W.; Boczkowska, A.; Ciecierska, E. *Polish J. Chem. Technol.* **2011**, *13*, 62.
45. Abdalla, M.; Dean, D.; Robinson, P.; Nyairo, E. *Polymer* **2008**, *49*, 3310.
46. Zhou, W.; Wang, J. J.; Gong, Z. L.; Gong, J.; Qi, N.; Wang, B. *Appl. Phys. Lett.* **2009**, *94*, 021904.
47. Nie, Y.; Hubert, T. *Polym. Int.* **2011**, *60*, 1574.
48. Cho, J.; Daniel, I. M.; Dikin, D. A. *Compos. A* **2008**, *39*, 1844.
49. Chen, W. J.; Li, Y. L.; Chiang, C. L.; Kuan, C. F.; Kuan, H. C.; Lin, T. T.; Yip, M. C. *J. Phys. Chem. Solids* **2010**, *71*, 431.
50. Arronche, L.; Gordon, K.; Ryu, D.; Saponara, V. L.; Cheng, L. J. *J. Mater. Sci.* **2013**, *48*, 1315.
51. Guo, X.; Yu, D.; Wu, J.; Min, C.; Guo, R. *Polym. Eng. Sci.* **2013**, *53*, 370.
52. Tsuchida, A.; Yoshimi, H.; Kiriyama, S.; Ohiwa, K.; Okubo, T. *Colloid Polym. Sci.* **2003**, *281*, 760.
53. Freed, L. E.; Hollander, A. P.; Martin, I.; Barry, J. R.; Langer, R.; Novakovic, G. V. *Express Cell Res.* **1998**, *240*, 58.
54. Infanger, M.; Kossmehl, P.; Shakibaei, M.; Bauer, J.; Kossmehl-Zorn, S.; Cogoli, A.; Curcio, F.; Oksche, A.; Wehland, M.; Kreutz, R.; Paul, M.; Grimm, D. *Cell Tissue Res.* **2006**, *324*, 267.
55. Fujiwara, Y.; Katsumoto, Y.; Ohishi, Y.; Koyama, M.; Ohno, K.; Akita, M.; Inoue, K.; Tanimoto, Y. *J. Phys. Conf. Ser.* **2006**, *51*, 458.
56. Beaugnon, E.; Tournier, R. *Nature* **1991**, *349*, 6309.
57. Yin, D. C.; Lu, H. M.; Geng, L. Q.; Shi, Z. H.; Luo, H. M.; Li, H. S.; Yea, Y. J.; Guo, W. H.; Shang, P.; Wakayamad, N. I. *J. Crystal Growth* **2008**, *310*, 1206.
58. Visco, A.; Calabrese, L.; Milone, C. *J. Reinf. Plast. Compos.* **2009**, *28*, 937.
59. Li, D. F.; Liu, Y. Y.; Kang, H. J.; Tan, H. F. *Adv. Mater. Res.* **2013**, *750–752*, 789.
60. Hameed, N.; Sreekumar, P. A.; Valsaraj, V. S.; Thomas, S. *Polym. Compos.* **2009**, *30*, 982.
61. Montazeri, A.; Khavandi, A.; Javadpour, J.; Tcharkhtchi, A. *Mater. Des.* **2010**, *31*, 3383.
62. Wang, B.; Gong, W.; Liu, W. H.; Wang, Z. F.; Qi, N.; Li, X. W.; Liu, M. J.; Li, S. J. *Polymer* **2003**, *44*, 4047.